Transverse detection of DNA using a MoS_2 nanopore

Michael Graf,[*,†] Martina Lihter,[†] Damir Altus,[‡] Sanjin Marion,[†] and Aleksandra Radenovic[*,†]

†*Laboratory of Nanoscale Biology, Institute of Bioengineering, School of Engineering, EPFL, 1015 Lausanne, Switzerland*

‡*Institute of Physics, HR-10000 Zagreb, Croatia*

E-mail: michael.graf@epfl.ch; aleksandra.radenovic@epfl.ch

Abstract

Classical nanopore sensing relies on the measurement of the ion current passing through a nanopore. Whenever a molecule electrophoretically translocates through the narrow constriction, it modulates the ion current. Although this approach allows to measure single molecules, the access resistance limits the spatial resolution. This physical limitation could potentially be overcome by an alternative sensing scheme taking advantage of the current across the membrane material itself. Such an electronic readout would also allow better temporal resolution than the ionic current. In this work, we present the fabrication of an electrically contacted molybdenum disulfide (MoS_2) nanoribbon integrated with a nanopore. DNA molecules are sensed by correlated signals from the ionic current through the nanopore and the transverse current through the nanoribbon. The resulting signal suggests a field-effect sensing scheme where the charge of the molecule is directly sensed by the nanoribbon. We discuss different sensing schemes such as local potential sensing and direct charge sensing. Furthermore, we

show that the fabrication of freestanding MoS_2 ribbons with metal contacts is reliable and discuss the challenges that arise in the fabrication and usage of these devices.

Keywords

field-effect transistor, DNA detection, nanopore, nanoribbon, molybdenum disulfide, MoS_2

Introduction

Solid-state nanopores have become a versatile tool to analyze single-molecules of deoxyribonucleic acid (DNA), proteins, and DNA-protein complexes.[1–5] A small hole in a thin membrane, typically in silicon nitride (SiN_x), provides the only connection between two compartments filled with saline solution. Applying a transmembrane voltage generates an electric field around the nanopore, which captures charged molecules that are freely diffusing in solution and electrophoretically drives them through the pore. During this translocation event, the ionic current is modulated as a function of the size, shape and charge of the molecule. Ultrathin membranes based on graphene,[6–8] MoS_2,[1,9] and hBN[10] have been investigated as a mean to provide a spatial resolution that approaches the distance between two bases of DNA. However, the sensing length of a nanopore in an ultrathin material does not correspond to the physical thickness of the membrane, due to a dominating contribution of the access resistance.[11] This physical limit is common to all ionic current measurements in solid-state nanopores and originates from the passage of ions from the bulk to the confined space of the nanopore. Furthermore, the noise of ion current measurements is very sensitive to the substrate and the membrane material and prohibits measurements at high temporal resolutions typically needed to detect small analytes such as proteins.[12] To overcome these limitations and to pave the way for ultrafast DNA sequencing using solid-state nanopores, a different approach is needed. Extending the existing ionic current sensor with an independent readout system would not render the nanopore obsolete but merely change

its function. In this case, the nanopore acts as a localizer, bringing single-molecules from free diffusion in solution to a well-defined location. For instance, combining nanopores with fluorescently tagged analytes provides an optical readout system, where the responsibility of the nanopore is solely the single-molecule loading of the analyte.[13–18] Another example was presented by Larkin et al,[19] where nanopores placed on the bottom of optical cavities improve the single-molecule real-time (SMRT) DNA sequencing by voltage-induced DNA loading.[19] In conventional nanopore devices based on ionic-current detection, nanopores need to be electrically insulated from each other, which is achieved by designing individual microfluidic channels. With an independent read out system this would not be required anymore, which would simplify the design and enable extremely dense packing.

Recently, two alternative approaches have been addressed in the literature: tunneling electrodes and field-effect sensing. Electrodes that attempt to measure the tunneling current across translocating nucleotides were first theoretically investigated by Zwolak et al.[20] Electrodes need to be placed immediately at the nanopore mouth to achieve the small distance needed for electron tunneling to work (2.5 nm).[21–23] Even though nanofabrication methods have improved substantially over the years, it is still extremely challenging to achieve the precision needed using conventional nanofabrication methods. One possible approach that, in the future, might allow to create tiny nanogaps is the use of break junctions through mechanically bending the substrate.[24–28]

The first field-effect inspired nanopore sensor was made from silicon nanowires and demonstrated that the local potential around a nanopore can be measured during DNA translocation.[29] When graphene emerged, it sparked substantial interest as a membrane material in nanopore sensors.[6–8] In contrast to a SiN_x membrane, the graphene membrane is a conductor and thus allows transversal current flow. The possibility of measuring simultaneously the ionic current and the sheet current through graphene lead to the creation of hybrid devices combining ionic sensing with transverse current. Contrary to the electrical gate of a classical field-effect transistor (FET), DNA is used to gate the device. Graphene

can acquire a bandgap when sculpted into a nanoribbon, becoming an ambipolar FET.[30] Different research groups have attempted to measure simultaneously the ionic current and the graphene sheet current during DNA translocations.[31–33] However, difficulties in the fabrication of the nanoribbons, device yield, and capacitive cross-talks[32] have severely limited the use of these sensors. When MoS_2 was first introduced as a membrane material for nanopore experiments,[1] the intrinsic bandgap of the material[34] has drawn the attention of theoreticians for its potential use of the sheet current for DNA sequencing.[35,36] When compared to single-layer graphene based biosensors, the MoS_2 based sensors are substantially more sensitive in detecting biomolecules,[37] emphasizing the potential practicality of this intrinsic semiconductor.

In this paper we present the implementation of a single-layer MoS_2 based FET device with a nanopore delivering molecules to the sensing region. We show translocation events that are simultaneously provoking an ionic current signature as well as a field-effect modulation. These transverse current signals caused by a field-effect modulation could potentially be explained by different sensing mechanisms. We estimate the expected signal for two sensing hypotheses and discuss which is the most likely mechanism by which the molecules are detected.

Results

A schematic representation of the proposed nanopore-FET device and the equivalent electronic circuit is depicted in Figure 1a-b. The goal was to design a narrow ribbon of MoS_2 (500 nm x 2 µm) on top of an aperture in a SiN_x membrane, as previously described.[38] The ribbon is then contacted with metal leads to provide the source and the drain. A dielectric material is deposited on the metal to electrically insulate these contacts from the electrolyte solution. Such a dielectric layer (20 nm of HfO_2) limits the cross-talk induced by capacitive coupling[32] and limits any electrochemical reaction between the metal and the electrolyte, as

well as the leakage of current between the source drain leads. A graphical summary of all the fabrication steps can be found in Supporting Figure 1. Figures 1c-e show representative transmission electron microscopy (TEM) images of finished devices, illustrating the successful fabrication process. To increase the yield of the devices, we fabricate three ribbons per membrane, from which only one (the ribbon in the middle, Figure 1c) has a freestanding part (suspended over the aperture in the SiN_x membrane). If the fabrication of the main ribbon (middle) fails, one of the two supported ribbons can be used for experiments in a supported configuration. Suspending the MoS_2 over an aperture has two reasons: first, the ultrathin nature of the MoS_2 membrane allows for very high signal-to-noise ratios when using the ionic current. Second, the thinner the membrane and the smaller the nanopore the larger the drop in local potential, provoked by DNA translocations, becomes.[39] The FET will, therefore, benefit from larger conductance modulations and the chances of detecting translocation events will be increased. The presence of the DNA inside the pore modifies the local potential distribution, such that in ideal conditions (pore diameter, $D = 1.3\,\mathrm{nm}$ and membrane thickness, $L = 0.6\,\mathrm{nm}$) the potential at the sensing area can be changed by up to $100\,\mathrm{mV}$ for a bias ionic voltage of $500\,\mathrm{mV}$.[39]

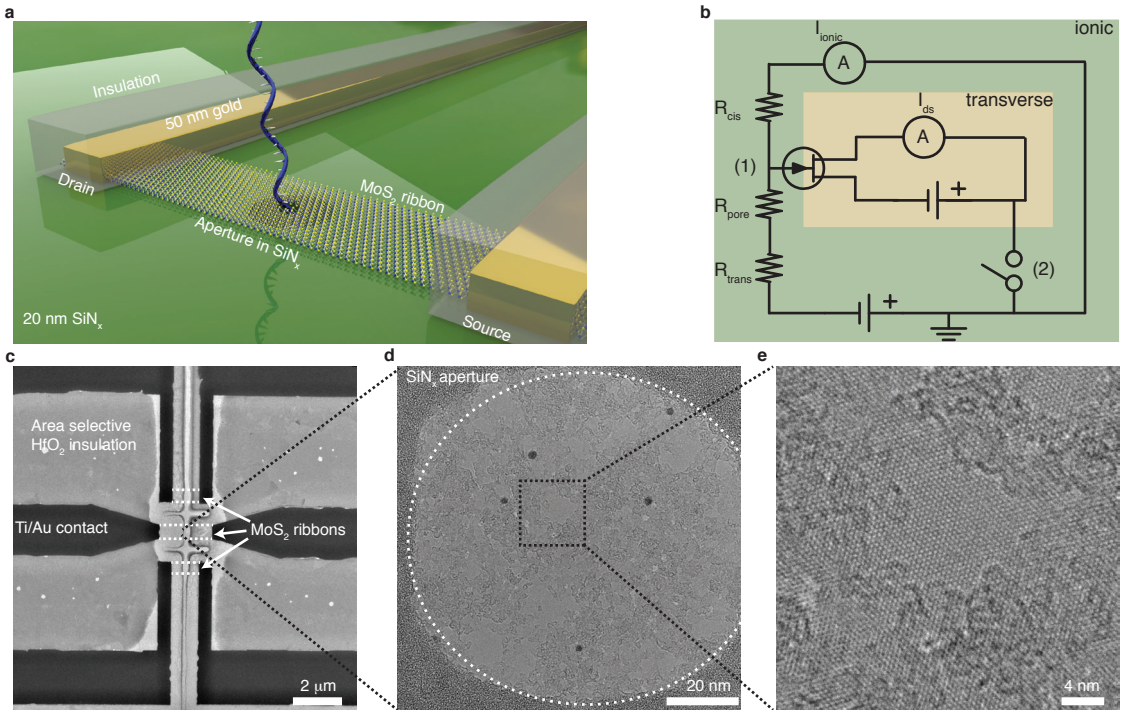

Figure 1: **Device overview.** **a**, A schematic of the proposed FET-nanopore device. Metal leads contact the monolayer MoS_2 crystal, which is subsequently etched into a ribbon. Area selective insulation around the electrodes avoids cross-talk and insulates the metal from the electrolyte while keeping the ribbon exposed to the liquid. An aperture in the SiN_x membrane provides a part where the MoS_2 is freestanding. Finally, a nanopore can then be drilled through the freestanding part using a TEM. The translocating DNA will then simultaneously modulate the ionic current as well as the transverse current. **b**, The equivalent electrical circuit describing the two subcircuits, denoted here as ionic and transverse. The MoS_2 ribbon is represented by a transistor at the vicinity of the nanopore (1). The switch symbol (2) denotes an optional decoupling of the two grounds. **c**, A TEM image of a finished device. Three ribbons are placed on the SiN_x membrane. The middle ribbon contains a suspended part. **d**, The suspended part of the middle ribbon. Crystalline monolayer MoS_2 is visible, surrounded by patches of poly(methyl methacrylate) (PMMA) residues. **e**, Clean parts of freestanding MoS_2 can be obtained even after multiple fabrication steps.

To confirm that the devices are functional, we perform an electrical characterization in dry condition. The conductance of MoS_2 ribbons is relatively low in air (about 100 pS), but can be pushed to high values in vacuum and thermal annealing (about 2 µS). The results of the electrical characterization can be found in Supporting Text 1.1.1 and Supporting Figure 2. Consistent with previous reports that MoS_2 behaves like a n-type semiconductor,[34] we observe that the conductance of the MoS_2 nanoribbon increases while applying positive

transmembrane potentials with respect to the ground (see Supporting Figure 3).

DNA translocations

Freestanding MoS_2 ribbons have limited stability when simultaneously measuring ionic and transverse currents. Uncontrolled electrical discharges on the drain-source contacts towards the Ag/AgCl electrodes in solution can potentially induce breakage of the MoS_2 membrane. To create a more stable device configuration for DNA translocation, we used one of the supported nanoribbons and drilled a nanopore through the MoS_2 and sequentially through SiN_x using a TEM (Figure 2a). We first measured the ionic conductance of the MoS_2-SiN_x nanopore in 1 M potassium chloride (KCl). The conductance obtained from the I-V characteristic (Figure 2b) corresponds well to the pore size observed in the TEM.[40] Next, we sweep the drain-source voltage to probe the MoS_2 ribbon current in 1 M KCl (Figure 2c). A ribbon conductance of 1 µS is observed. In the absence of DNA, we observe neither ionic nor transverse current blockages. Next, we added 80 nucleotides (nt) long single-stranded DNA (ssDNA) and simultaneously record the ionic and transverse current. Distinct current drops with about 15 % blockage are visible on the ionic current trace. At 1 M KCl only short spikes were visible on the transverse channel, correlating with the events observed in the ionic current trace. Figure 2d shows a representative sample of 15 events (raw continuous traces for all sensing experiments are available in Supporting Figure 4). To increase the local potential and the Debye length around the nanopore, we lowered the salt concentration to 10 mM / 100 mM. Correlated signals started to appear on the transverse current. We recorded a total of 759 correlated events. Figure 2e shows a representative collection of 15 recorded events. The ionic events mainly consist of a current decrease followed by a very short current increase. This is consistent with previous work in low-salt concentration, where the initial dip in current is assigned to access resistance probing and the current overshoot is assigned to an increase of ions inside the nanopore due to mobile counterions along the DNA molecule. This overshoot is associated with the translocation.[41,42] The current decrease on

the transverse channel is perfectly correlated to the part where the DNA probes the access resistance and returns back to the baseline once the translocation starts.

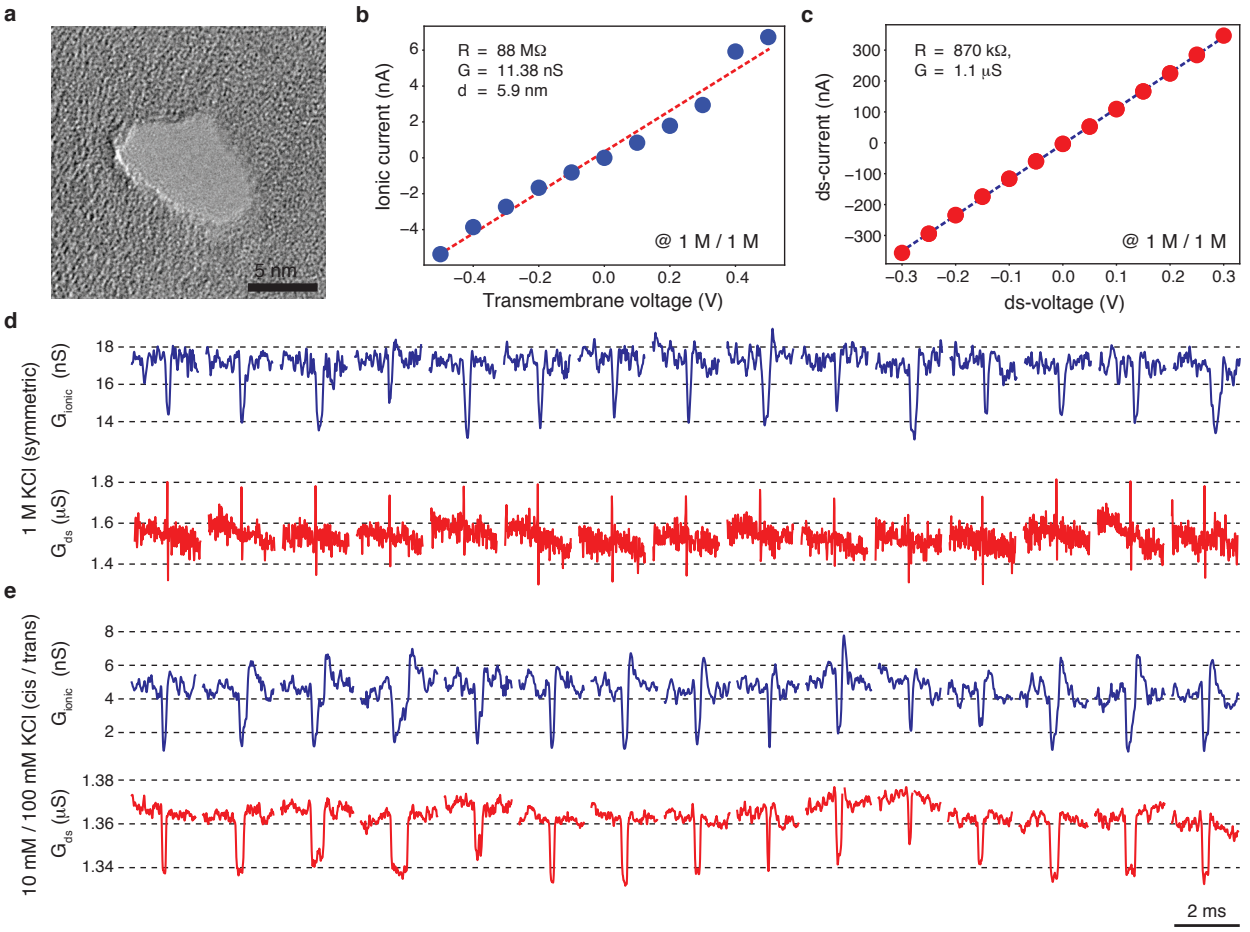

Figure 2: **Experimental data of 80 nt ssDNA translocation with common ground.** **a**, A TEM image of the nanopore drilled through MoS_2 and the SiN_x membrane. **b**, Ionic I-V performed at 1 M KCl confirming the pore size obtained in **a**. **c**, Drain-source current (I_{ds}) vs. drain-source voltage (V_{ds}) at 1 M KCl. **d**, Concatenated signal traces representative of the dataset at 1 M KCl. **e**, Concatenated signal traces representative of the dataset at 10 mM / 100 mM (*cis*/*trans*) KCl. Both channels were sampled at 100 kHz and digitally low-pass filtered at 15 kHz.

Previous reports of transverse currents in graphene nanoribbons have shown strong derivative signals on the sheet current, induced by the ionic signal.[32] Although the data presented in Figure 2e does not resemble the derivative signals reported, some cross-talk could still occur if the insulation layer is not sufficient (see Supporting Text 1.2). For in-

stance, on one device (Supporting Figure 5a and b) with poor insulation, current leakages between the two channels occurred (Supporting Figure 5c). To completely eliminate this possibility, we developed a novel electronic circuit based on a differential amplifier, which decouples and electrically insulates the two circuits, similarly to the set-up presented in Heerema et al.[33] This electronic set-up provides a strong insulation between the two measurement circuits of up to 75 GΩ. All details on the design and the performance of the circuit can be found in Supporting Text 1.3 and Supporting Figure 6a-c. The new electronic set-up was then used to test analytes of different charge polarities to probe their gating capabilities on the FET. We translocated analytes with neutral, positive and negative charges in a device with a small nanopore of about 2.5 nm in diameter in a supported nanoribbon (see Supporting Figure 7 for TEM images): 1 kilobase pairs (kbp) double-stranded DNA (dsDNA) (negative), polylysine (positive, average molecular weight (mw): 30×10^3 - 70×10^3 $\mathrm{g\,mol^{-1}}$) and polyethylene glycol (PEG) (neutral, average mw: 20×10^3 $\mathrm{g\,mol^{-1}}$). All measurements were done in a concentration gradient of 10 mM / 1 M. Figure 3a reports the correlated signals obtained when translocating 1 kbp dsDNA. Consistent with the previous measurement (ssDNA, Figure 2), the negatively charged DNA molecules induce decreases of the drain-source conductance of the FET. After carefully washing the flow-cell the neutrally charged PEG molecules were added. These molecules cannot be translocated electrophoretically, we therefore exploit the electroosmotic flow to drag the molecules through the orifice. Strong ionic conductance decreases indicate successful translocations of PEG molecules (Figure 3b). However, most of the time no transverse signals were visible. Unlike the small size biological pores that allow for the PEG to be unfolded, in our system it is very likely that PEG translocates in a partially folded state leading to large conductance drops. Last, the positively charged polylysine molecules were added. During translocation of polylysine the ionic signal is showing short conductance decreases, whereas the transverse signal shows conductance increases Figure 3c.

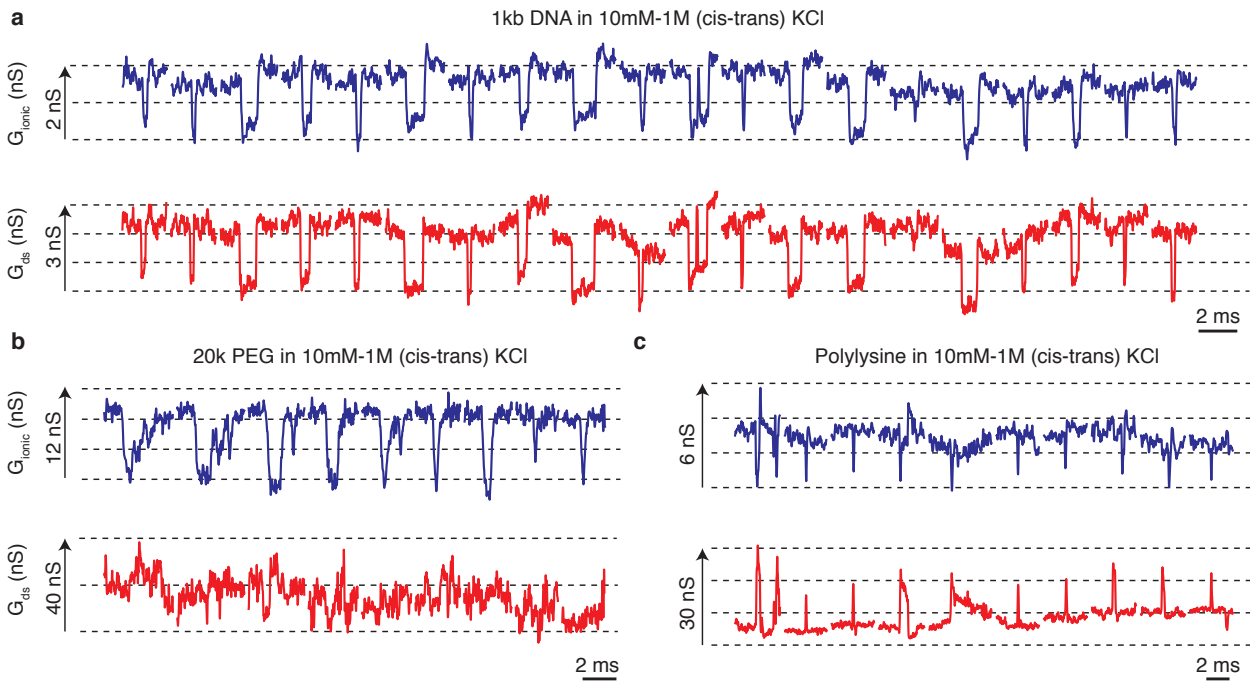

Figure 3: **Translocation data for differently charged analytes.** **a**, 1 kbp dsDNA translocations. **b**, PEG ($\mathrm{mw} = 20 \times 10^3\,\mathrm{g\,mol^{-1}}$) translocations. **c**, Translocations of polylysine molecules. Both channels were sampled at 100 kHz and digitally low-pass filtered at 15 kHz.

Discussion

Figure 4 shows the current-drop versus dwell-time scatter plots of the ionic signal (Figure 4a) and the the drain-source current (Figure 4b). There are no distinct subpopulations visible in the distributions of the current drops in the ionic channel and the drain-source channel. The dwell time shows a log-normal distribution suggesting that very short events are missed.[12] Furthermore, both the amplitudes of the current drops and dwell times observed correlate very well between the two channels (Pearson's correlation coefficient of 0.7 and 0.63 respectively, Figure 4c and d). The correlation of the amplitudes of the two signals suggest a common physical origin.

Initially, we were puzzled by the relative long dwell times of 80 nt ssDNA (the average dwell time is about 200 µs). However, previous studies have found long passage times of 50

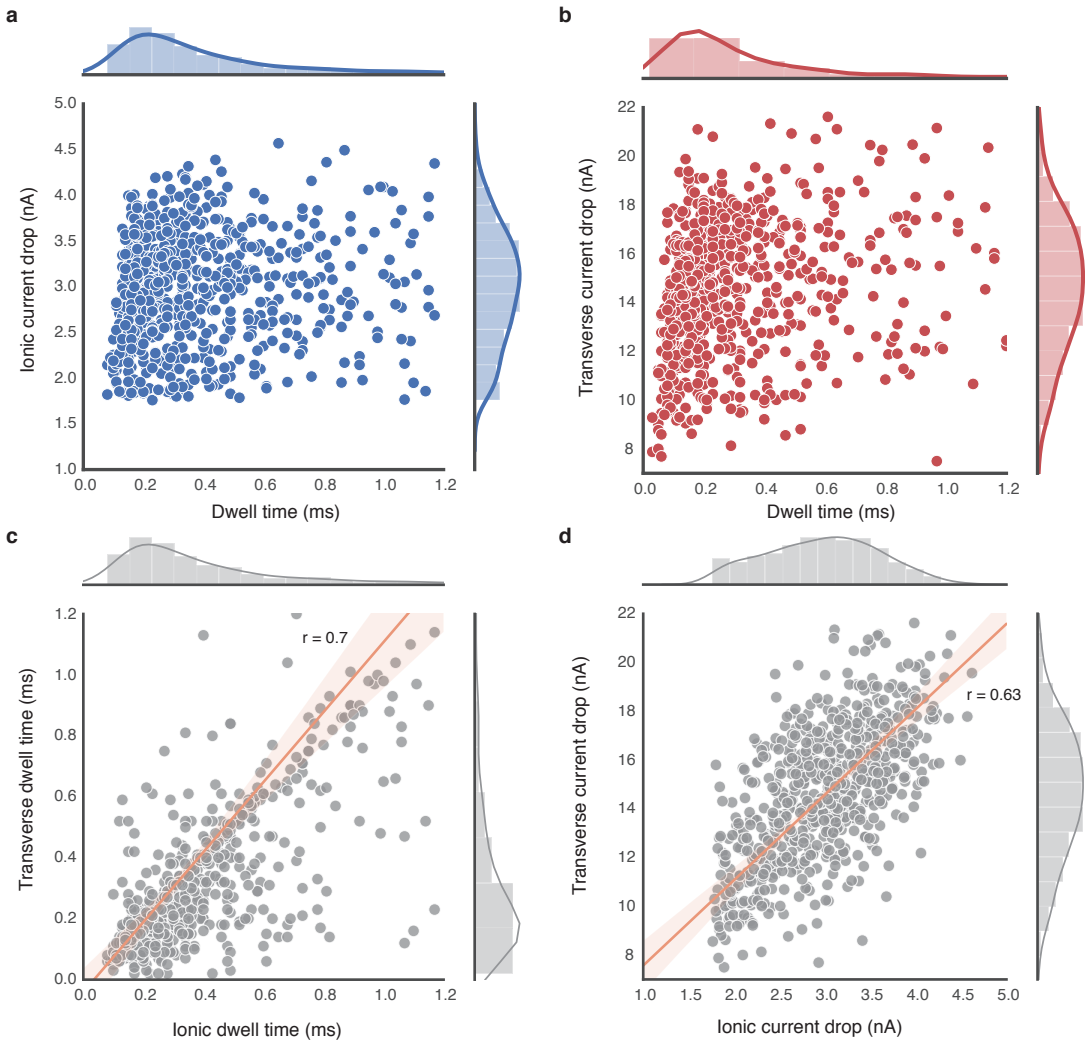

Figure 4: **Scatter plots of the translocations reported in Figure 2**. **a**, Current drop versus the dwell time for the translocations recorded in the ionic channel. **b**, Current drop versus dwell time for the translocations recorded in the transverse channel. **c**, Correlation between the dwell times of the transverse and the ionic channels. **d**, Correlation between the current drops of the transverse and the ionic channels. n = 759

nt ssDNA in gold-coated pores. This effect was explained by physisorption of bases with the gold surface.[43,44] A similar mechanism occurs on the MoS_2 membrane, where Van der Waals forces between the nucleobases and the basal plane of MoS_2 are responsible for the interaction.[45] Lower adsorption is found for dsDNA.[45] Further, molecular dynamics (MD) simulations have shown that ssDNA can interact with a MoS_2 surface, whereas dsDNA shows nearly no sticking behaviour.[46]

Sensing scheme

In nanopore devices coupled with transverse sensing, capacitive coupling and electrostatic gating can produce transverse signals. Capacitive coupling is a current induced at electrodes close to the nanopore, which results in time-derivative signals that are not proportional to the ionic current drop.[32,33] While, electrostatic gating, on the other hand, causes a field-effect on the transistor that is proportional to the ionic current drop.[29] In our experiments, we see a proportionality between the transverse and the ionic current drops (Figure 4d). Furthermore, we observed a dependence of transverse signal on the screening length (Figure 2d-e) and the charge of the molecule (Figure 3). Lastly, we did not observe any time-derivative signal on the transverse channel for devices with well isolated metal contacts.[47] For these reasons, we propose that electrostatic gating of the transistor is the most probable underlying physical principle. Here we discuss, on the phenomenological level, two main contributions to the electrostatic gating of the transistor: gating due to a change in the local potential at the nanopore during DNA translocation and gating by the charge of the translocating molecule. In the literature, a local potential change due to DNA insertion is most frequently used to explain the observed current change.[29,31] However, only Xie et al. were able to investigate the behavior of their system careful enough to make a conclusion on the most likely sensing principle. Heerema et al. discuss that the direct sensing of the charge of the DNA backbone could also explain their experimental data.[33] Following the same approach as in Heerema et al.,[33] we compare the expected current changes for the two main contributions and we determine the dominant one.

Change in the local potential due to a translocation

In this scheme the translocation of a molecule generates an electric field drop around the nanopore, which effectively gates the FET. The experimental data reported in Figure 2 shows a clear dependence of the transverse signal on the salt concentration. As previously explained by Xie et al., in 1 M / 1 M KCl the electric field drops symmetrically at the

nanopore (see Supporting Figure 3b), whereas concentration gradients, such as 10 mM / 100 mM enlarge the resistance in one compartment, extending the electrical field drop further into the *cis*-chamber, as shown in the finite element model (FEM) simulations of the potential distribution (Supporting Figure 3c). Therefore, the translocation of DNA induces potential changes at distances further away from the nanopore. This effectively gates a larger surface of the ribbon. We can estimate the expected drain-source current change by following the analysis proposed by Parkin et al.[39] The current drop ΔI_{ds} on the FET can be described by:

$$\Delta I_{\mathrm{ds}} = g_{\mathrm{eff}} \Delta V_{\mathrm{molecule}} \tag{1}$$

, where g_{eff} is the effective transconductance at the nanopore and $\Delta V_{\mathrm{molecule}}$ is the voltage change induced by the translocating molecule. The effective transconductance scaled with the access resistance at the entrance of the pore can be expressed as:[39] $g_{\mathrm{eff}} = \frac{dI_{\mathrm{ds}}}{dV_{\mathrm{en}}}$, where I_{ds} is the drain-source current and V_{en} is the potential at the pore entrance. Using the potential distribution calculated in Supporting Figure 3c, we can estimate $V_{\mathrm{en}} \approx \frac{3}{5} V_{\mathrm{tm}}$, where V_{tm} is the applied transmembrane voltage. The supported nanoribbon used to produce the data in Figure 2 showed very weak dependence on the transmembrane voltage. This might be due to the screening of the electric field by the silicon nitride membrane. We assume a transconductance value of $g_{\mathrm{eff}} \approx 5\,\mathrm{nS}$ (Supporting Figure 8). We can then calculate the effective transconductance as: $g_{\mathrm{eff}} = \frac{dI_{\mathrm{ds}}}{\frac{3}{5} dV_{\mathrm{tm}}} = \frac{5}{3} \cdot 5\,\mathrm{nS} = 8.3\,\mathrm{nS}$. An absolute upper limit for the potential change induced by the translocation of DNA can be fixed to 100 mV.[39] Then the expected current change in the FET is $I_{\mathrm{ds}} = 100\,\mathrm{mV} \cdot 8.8\,\mathrm{nS} \approx 0.8\,\mathrm{nA}$, which cannot be resolved given the high noise of our device (Supporting Figure 9). However, this approach neglects the charge of the molecule itself and attributes the voltage changes solely to the perturbation of the electric field due to the presence of DNA. Additionally, it fails to explain the absence of a transverse signal when the uncharged PEG molecules are translocated (Figure 3b).

Contribution from the charge of the translocating molecule

Here, we hypothesize that only the charge of the molecule gates the transistor and focus on the translocation of DNA molecules. Monolayer MoS_2 typically behaves like a n-type FET.[34] The charge of the DNA backbone is negative, and we would, therefore, expect a drop in the drain-source current of the MoS_2-FET. The absence of any FET-signal at a salt concentration of 1 M KCl can be explained by a strong charge screening. In water, the distance at which electrostatic effects persist can be expressed by the Debye length, estimated through $\lambda_D = \frac{3.04 \cdot 10^{-10}}{\sqrt{c}}$, where c is the KCl concentration.[48] In 1 M KCl the Debye length is roughly 0.3 nm, whereas, at the more dilute 10 mM case, the Debye length extents to 3 nm.[48] The charge of the DNA backbone has, therefore, an effect on a larger surface of the ribbon. Another factor to consider is the interaction of ssDNA on the MoS_2 surface. MD simulations have shown that ssDNA as opposed to dsDNA can adsorb on the MoS_2 surface through Van der Waals forces, starting with the adsorption of the two ends.[46] This Van der Waals forces combined with the electrophoretic force immobilizes the ssDNA shortly before being dragged through the nanopore by the electric field. During that time, a large amount of the DNA molecule is in close contact with the MoS_2 ribbon, effectively gating the transistor and provoking the transverse current decrease observed. Brownian motion then jiggles the molecule trapped by the electrophoretic force until the DNA molecule can translocate. This increases the ion concentration in the pore by bringing additional counterions (visible as an overshoot in the ionic current).[41] While the DNA is inside the nanopore it is invisible to the MoS_2-FET as all the charges are screened by the SiN_x layer. The current change due to the charge of a molecule can be estimated using the capacitance of the MoS_2-liquid interface C_i per area and the effective charge of the molecule Q_{eff} acting on a surface A, using the following relationship:[33]

$$\Delta I_{\text{ds}} = g_{\text{eff}} \frac{Q_{\text{eff}}}{C_i A} \tag{2}$$

We can roughly estimate the capacitance C_i by combining the contribution of the electrical double layer (EDL), C_{EDL} and the quantum capacitance C_q:[49]

$$\frac{1}{C_i} = \frac{1}{C_q} + \frac{1}{C_{\mathrm{EDL}}} = \frac{C_{\mathrm{EDL}} + C_q}{C_{\mathrm{EDL}} C_q} \tag{3}$$

Combining Equations 3 and 2 yields the final expression of the expected current drop ΔI_{ds}:

$$\Delta I_{\mathrm{ds}} = g_{\mathrm{eff}} \frac{Q_{\mathrm{eff}}(C_{\mathrm{EDL}} + C_q)}{C_{\mathrm{EDL}} C_q A} \tag{4}$$

The quantum capacitance in 2D-systems can be calculated using the relationship:[49] $C_q = \frac{e^2 m^*}{\pi \hbar^2}$, where $\hbar$ is the reduced Planck constant, e the elementary charge and m^* the rest mass of an electron. The value of the quantum capacitance is therefore: $C_q = 0.67\,\mathrm{F\,m^{-2}}$.

The capacitance due to the EDL can be estimated through: $C_{\mathrm{EDL}} = \frac{\epsilon\epsilon_0}{\lambda}$, where $\lambda = 3\,\mathrm{nm}$ is the Debye length at 10 mM KCl,[48] ϵ_0 the permittivity of vacuum and $\epsilon \approx 80$, the permittivity of the electrolyte used. This results in a value for the EDL capacitance as: $C_{\mathrm{EDL}} = 0.24\,\mathrm{F\,m^{-2}}$. Using Equation 3, we can calculate the total capacitance to be $C_i = 0.17\,\mathrm{F\,m^{-2}}$. Using the transconductance of the device used to measure the data presented in Figure 2 ($\approx 5.3\,\mathrm{nS}$), we can estimate the expected current change through Equation 4: $\Delta I_{\mathrm{ds}} \approx 4.8\,\mathrm{nA}\,e^{-1}\,\mathrm{nm^{-2}}$. Theoretically, the 80 nt long ssDNA used in the first experiment (Figure 2) should have a charge of $80\,e$. The experimental data contains typical current drops of about 15 nA, suggesting that about 3 to 4 elementary charges are sensed per nm^2. The only value that can vary is the capacitance of the EDL. The expected current-drop is therefore proportional to the Debye length and inversely proportional to the dielectric constant of the solvent: $\Delta I_{\mathrm{ds}} \propto \frac{\lambda}{\epsilon\epsilon_0}$. For example, in 1 M KCl, the Debye length is only 0.3 nm,[48] which would lead to an expected current drop of $\Delta I_{\mathrm{ds}} \approx 1\,\mathrm{nA}\,e^{-1}\,\mathrm{nm^{-2}}$. This could potentially explain the absence of a substantial transverse signal in high-salt conditions.

Judging from the results of the calculations for the two contributions it is obvious that

direct charge sensing can induce larger conductance modulations compared to the contribution that originates from the local potential change due to the insertion of the molecule to the pore. The data presented in Figure 2 shows that the amplitude of the obtained conductance decreases are realistic within the direct charge sensing scheme. Furthermore, the data presented in Figure 3 confirms the charge dependence of the field-effect modulation of the transistor. Consistent with an n-type FET behaviour, a conductance increase is observed when polylysine molecules translocate across the nanopore (Figure 3c). Similarly, when the translocating molecule does not possess any charge, the FET is not gated (Figure 3b). We thus conclude that direct charge sensing is the most probable sensing mechanism.

Noise

The question remains whether the transverse channel can actually provide an improved signal compared to the ionic channel. To estimate the potential improvements of the transverse sensing scheme we can compare the signal-to-noise ratio (SNR) values between the signals of the two channels (data from Figure 2). To compare the signal between the channels, we digitally filtered the transverse signal to match the low-pass cutoff of 10 kHz of the ionic channel before calculating the SNR values. The SNR was defined as: $\mathrm{SNR} = \frac{\Delta I}{\sigma_{\mathrm{baseline}}}$, where ΔI is the observed current drop and $\sigma_{\mathrm{baseline}}$ the standard deviation of the baseline upstream of the current drop. Supporting Figure 10 shows the probability density function (PDF) and boxplots of the two cases. The transverse current has a 40 % higher SNR. The median of the SNR of all 759 correlated events presented in Figure 2 is 7.7 for the ionic current and 10.7 for the transverse current. This increase in SNR illustrates the potential improvements that the transverse measurement scheme can offer and could pave the way to higher bandwidth recordings, where noise typically masks translocation events.

The simultaneous measurement of the ionic and transverse circuit increases the noise of the system. Supporting Figure 9 shows the power spectral density as well as typical baseline values of the two channels in high-salt (1 M / 1 M KCl) and low-salt condition (10 mM /

100 mM KCl). The standard deviation of the ionic current increases in low-salt from 0.5 nA to 0.8 nA. The noise on the transverse current, however, decreases substantially from 8.6 nA to 3.1 nA. The increase of the ionic noise with lower salt concentration is consistent with previous reports[50] and is associated with the low-frequency 1/f noise that scales inversely with the number of charge carriers.[50] On the transverse channel, a strong noise reduction is observed with lower salt concentration, which is in contrast to the graphene-FET device presented by Puster et al.,[32] where the noise on the transverse channel increased with lower salt concentrations.

Yield

We faced several fabrication-related challenges, which are described in detail in Supporting Text 1.2. In total, we fabricated approximately 200 devices. The fabrication of about 100 devices was needed to optimize the fabrication process. After optimization, about 50 devices reached the final fabrication step. Most devices were eliminated during the process due to breakage of the SiN_x membrane or problems during metal lift-off. Out of these 50, only about 20 devices were clean enough and had intact ribbons (characterized with a TEM images). Often, cracks in the nanoribbons interrupted the current flow (Supporting Figure 11). Another common issue is contaminations in the vicinity of the aperture, likely due to the reactive ion etching (RIE) and potassium hydroxide (KOH) etching processes (Supporting Figure 12). Lastly, devices with clean freestanding MoS_2 layers tend to break rapidly once both measurement channels were connected, suggesting that large current discharges can occur. From these 20 devices, only 3 devices allowed the recording of translocation events. This low yield is consistent with previous efforts in fabricating nanopore-FET devices,[29,31–33] emphasizing the difficulty of the fabrication process.

Conclusion

We have shown that the fabrication of freestanding MoS_2 ribbons containing a nanopore is technically possible. However, the stability of freestanding ribbons when both measurement channels were connected remains to be solved. By using supported MoS_2 ribbons, we have shown that correlated transverse signals can be obtained. Ionic signals are highly dominated by capacitive noise at higher frequencies, the FET measurement scheme could, therefore, be beneficial to achieve high signal-to-noise ratios at bandwidths up to 100 MHz.[39] By pushing more charge carriers into the conduction band, we believe that much higher signal-to-noise ratios are possible. Therefore it is crucial to find a suitable method to gate the ribbons to take full advantage of the field effect sensing capabilities of monolayer MoS_2.

The results presented show that direct charge sensing is the most probable sensing mechanism. To further boost the direct charge sensing, another solvent, such as room temperature ionic liquids could lower the dielectric constant ϵ and therefore increase the amplitude of the current modulation. For example, typical dielectric constant values of room temperature ionic liquids range between 10 to 20,[51] which could boost the current modulation to $\Delta I_{\mathrm{ds}} \approx 20\,\mathrm{nA}\,e^{-1}\,\mathrm{nm}^{-2}$. Additionally, recent experiments have revealed that room temperature ionic liquids (RTILs) have a remarkably long ranged screening length.[52]

The morphology of the two signals might allow us to decouple two distinct parts of the translocation process. Since the FET only senses the molecule when it is close to the MoS_2 surface, we can effectively only detect the moment before the translocation when the DNA is in close contact to the MoS_2 surface. Comparing the signals of the two channels might help to interpret the ionic current traces and decouple access resistance probing from the actual translocation. In contrast, by solving the problems associated with the stability of freestanding MoS_2layers, we can expect to probe the translocation process since the charge of the DNA would no longer be screened by a layer of SiN_x.

Methods

A detailed graphical summary of the fabrication procedure can be found in Supporting Figure 1. The basis of the device is a SiN_x membrane containing a 50 nm to 100 nm aperture created by e-beam lithography (EBL) (EBPG 5000ES, Vistec Electron Beam GmbH , Jena, Germany) and RIE (SPTS APS, Orbotech, Yavne, Israel) of the SiN_x layer. The exact procedure of creating the nitride membrane and the aperture can be found elsewhere.[38] On this hole, a chemical vapor deposition (CVD) grown (home-made system), single-crystal MoS_2 layer is transferred onto the aperture in a SiN_x membrane using a PMMA wet transfer approach described elsewhere.[38] The transferred monolayer is then contacted via Ti/Au electrodes by EBL and e-beam assisted metal evaporation. The crystal is then etched into a ribbon of 500 nm thickness and 2 µm length using EBL and RIE (O_2 gas) to restrain the current flow to the area of interest. An area selective insulation is then deposited on the metal leads using EBL and 20 nm thick HfO_2 grown by atomic layer deposition (ALD) (TFS200, BENEQ, Espoo, Finland). In all EBL steps, a three-step alignment scheme is used to achieve an alignment precision of less than 50 nm (Supporting Figure 13). A computer-aided design (CAD) summarizing the different fabrication steps can be found in Supporting Figure 14a and b. Finally, a TEM (FEI Talos, Thermo Scientific, Oregon, USA) is then used to drill a nanopore either into the suspended part of the crystal or through one of the supported backup-nanoribbons.

Just before the experiment, a silicone elastomer is painted around the membrane to reduce the capacitance of the chip and provide additional insulation between the metal leads and the electrolyte.

To connect the device to the macroscopic world, the fabricated chip is glued to a custom-made printed circuit board (PCB) using double-sided polyimide tape and sandwiched by a custom made PMMA flow-cell (Supporting Figure 14c). A thin cylindrical access-pillar brings the buffer to the nanopore device, while keeping the wires dry (Supporting Figure 14d). The PCB is then connected through a custom wired secure digital (SD) card connector

to the set-up.

1 kbp dsDNA was purchased from ThermoFisher Scientific (Waltham, United States) and 80 nt ssDNA was purchased from Microsynth (Balgach, Switzerland). PEG (average mw: 20×10^3 g mol^{-1}) and poly-D-lysine hydrobromide (average mw: 30×10^3 - 70×10^3 g mol^{-1}) were purchased from Sigma-Aldrich (St. Louis, United States).

The current measurements are performed using an Axopatch 200B (Molecular Devices, San Jose CA, USA) at 10 kHz low-pass to measure the ionic current and a Femto DLPCA-200 (FEMTO Messtechnik GmbH, Berlin, Germany) at 50 kHz low-pass to measure the transverse current across the membrane. Both amplifier outputs are then digitized at 100 kHz using a two-channel NI-PXI-4461 (National Instruments, Austin TX, USA). A custom written LabView (National Instruments, Austin TX, USA) program is used to apply the voltages and save the data. All data has been analyzed with custom made scripts using Python 3.7. The rendering of the schematics was done using Blender 2.79b.

Alignment of subsequent EBL steps

A three-step alignment is used in all EBL steps to precisely align the location of the aperture with the electrode deposition, the ribbon etching and the insulation (Supporting Figure 15). First, a pre-alignment marker containing an array of 50 µm squared pads at increasing distances of 1 µm is used to roughly align the 12 x 12 mm^2 sized substrate. Since every marker is at an increasing distance from its neighboring markers, the system can back-calculate the exact location of the center-marker from any three markers within the array. This greatly simplifies the manual alignment and measurements on the EBL holders. Second, alignment markers at each edge of the chip perform a global alignment by correcting for offset, scale, rotation, and keystone. Third, just before the pattern gets written, the last set of alignment markers just next to the SiN_x membrane is fine-tuning the alignment. This process allows alignment precisions greater than 50 nm judged by the shifts between the aperture in the SiN_x membrane and the MoS_2 nanoribbon (Supporting Figure 13a-c).

Acknowledgement

The authors thank D. Dumcenco for providing CVD-grown MoS_2, the center for micronanotechnology (CMi) for access and support of cleanroom equipment, and the interdisciplinary centre for electron microscopy (CIME) for access to TEM. The authors also thank Dmitry Ovchinnikov for help with vacuum measurements. The authors thank K. Liu, A. Sarathy, A. Descloux, M. Thakur, M. Zhang, J. Deen, J. Gundlach and J. P. Leburton for helpful discussions. This work was financially supported by the Swiss National Science Foundation (SNSF) Consolidator grant (BIONIC BSCGI0_157802) and by a sponsored research agreement from Hoffmann-LaRoche.

Supporting Information Available

The following files are available free of charge.

- SupportingInformation.pdf: Electronic Characterization, Fabrication Challenges, Differential Amplifier Circuit, Supporting Figures

References

(1) Liu, K.; Feng, J.; Kis, A.; Radenovic, A. Atomically thin molybdenum disulfide nanopores with high sensitivity for dna translocation. *ACS Nano* **2014**, *8*, 2504–2511.

(2) Larkin, J.; Henley, R. Y.; Muthukumar, M.; Rosenstein, J. K.; Wanunu, M. High-bandwidth protein analysis using solid-state nanopores. *Biophysical Journal* **2014**, *106*, 696–704.

(3) Yusko, E. C.; Bruhn, B. R.; Eggenberger, O. M.; Houghtaling, J.; Rollings, R. C.; Walsh, N. C.; Nandivada, S.; Pindrus, M.; Hall, A. R.; Sept, D.; Li, J.; Kalonia, D. S.;

Mayer, M. Real-time shape approximation and fingerprinting of single proteins using a nanopore. *Nature Nanotechnology* **2017**, *12*, 360–367.

(4) Kowalczyk, S. W.; Hall, A. R.; Dekker, C. Detection of local protein structures along DNA using solid-state nanopores. *Nano Letters* **2010**, *10*, 324–328.

(5) Raillon, C.; Cousin, P.; Traversi, F.; Garcia-Cordero, E.; Hernandez, N.; Radenovic, A. Nanopore detection of single molecule RNAP-DNA transcription complex. *Nano Letters* **2012**, *12*, 1157–1164.

(6) Schneider, G. F.; Kowalczyk, S. W.; Calado, V. E.; Pandraud, G.; Zandbergen, H. W.; Vandersypen, L. M. K.; Dekker, C. DNA Translocation through Graphene Nanopores. *Nano Letters* **2010**, *10*, 3163–3167.

(7) Garaj, S.; Hubbard, W.; Reina, A.; Kong, J.; Branton, D.; Golovchenko, J. A. Graphene as a subnanometre trans-electrode membrane. *Nature* **2010**, *467*, 190–193.

(8) Merchant, C. A.; Healy, K.; Wanunu, M.; Ray, V.; Peterman, N.; Bartel, J.; Fischbein, M. D.; Venta, K.; Luo, Z.; Johnson, A. T.; Drndić, M. DNA translocation through graphene nanopores. *Nano Letters* **2010**, *10*, 2915–2921.

(9) Feng, J.; Liu, K.; Bulushev, R. D.; Khlybov, S.; Dumcenco, D.; Kis, A.; Radenovic, A. Identification of single nucleotides in MoS_2 nanopores. *Nature Nanotechnology* **2015**, *10*, 1070–1076.

(10) Liu, K.; Lihter, M.; Sarathy, A.; Caneva, S.; Qiu, H.; Deiana, D.; Tileli, V.; Alexander, D. T. L.; Hofmann, S.; Dumcenco, D.; Kis, A.; Leburton, J.-P.; Radenovic, A. Geometrical Effect in 2D Nanopores. *Nano Letters* **2017**, *17*, 4223–4230.

(11) Hall, J. E. Access resistance of a small circular pore. *The Journal of General Physiology* **1975**, *66*, 531–532.

(12) Plesa, C.; Kowalczyk, S. W.; Zinsmeester, R.; Grosberg, A. Y.; Rabin, Y.; Dekker, C. Fast translocation of proteins through solid state nanopores. *Nano Letters* **2013**, *13*, 658–663.

(13) McNally, B.; Singer, A.; Yu, Z.; Sun, Y.; Weng, Z.; Meller, A. Optical Recognition of Converted DNA Nucleotides for Single-Molecule DNA Sequencing Using Nanopore Arrays. *Nano Letters* **2010**, *10*, 2237–2244.

(14) Soni, G. V.; Singer, A.; Yu, Z.; Sun, Y.; McNally, B.; Meller, A. Synchronous optical and electrical detection of biomolecules traversing through solid-state nanopores. *Review of Scientific Instruments* **2010**, *81*, 014301.

(15) Yamazaki, H.; Kimura, S.; Tsukahara, M.; Esashika, K.; Saiki, T. Optical detection of DNA translocation through silicon nanopore by ultraviolet light. *Applied Physics A* **2014**, *115*, 53–56.

(16) Assad, O. N.; Di Fiori, N.; Squires, A. H.; Meller, A. Two color DNA barcode detection in photoluminescence suppressed silicon nitride nanopores. *Nano Letters* **2015**, *15*, 745–752.

(17) Pitchford, W. H.; Kim, H. J.; Ivanov, A. P.; Kim, H. M.; Yu, J. S.; Leatherbarrow, R. J.; Albrecht, T.; Kim, K. B.; Edel, J. B. Synchronized optical and electronic detection of biomolecules using a low noise nanopore platform. *ACS Nano* **2015**, *9*, 1740–1748.

(18) Gilboa, T.; Torfstein, C.; Juhasz, M.; Grunwald, A.; Ebenstein, Y.; Weinhold, E.; Meller, A. Single-Molecule DNA Methylation Quantification Using Electro-optical Sensing in Solid-State Nanopores. *ACS Nano* **2016**, *10*, 8861–8870.

(19) Larkin, J.; Henley, R. Y.; Jadhav, V.; Korlach, J.; Wanunu, M. Length-independent DNA packing into nanopore zero-mode waveguides for low-input DNA sequencing. *Nature Nanotechnology* **2017**, *12*, 1169 EP –.

(20) Zwolak, M.; Di Ventra, M. Electronic signature of DNA nucleotides via transverse transport. *Nano Letters* **2005**, *5*, 421–424.

(21) Lindsay, S.; He, J.; Sankey, O.; Hapala, P.; Jelinek, P.; Zhang, P.; Chang, S.; Huang, S. Recognition tunneling. *Nanotechnology* **2010**, *21*, 262001.

(22) Carminati, M.; Ferrari, G.; Ivanov, A. P.; Albrecht, T.; Sampietro, M. Design and characterization of a current sensing platform for silicon-based nanopores with integrated tunneling nanoelectrodes. *Analog Integrated Circuits and Signal Processing* **2013**, *77*, 333–343.

(23) Fanget, A.; Traversi, F.; Khlybov, S.; Granjon, P.; Magrez, A.; Forr??, L.; Radenovic, A. Nanopore integrated nanogaps for DNA detection. *Nano Letters* **2014**, *14*, 244–249.

(24) Chidsey, C. E. D.; Tao, N. J. Free Energy and Temperature Dependence of Electron Transfer at the Metal-Electrolyte Interface. *Science* **1991**, *251*, 919–922.

(25) He, J.; Sankey, O.; Lee, M.; Tao, N.; Li, X.; Lindsay, S. Measuring single molecule conductance with break junctions. *Faraday Discuss.* **2006**, *131*, 145–154.

(26) Tsutsui, M.; Shoji, K.; Taniguchi, M.; Kawai, T. Formation and self-breaking mechanism of stable atom-sized junctions. *Nano Letters* **2008**, *8*, 345–349.

(27) Tsutsui, M.; Taniguchi, M.; Kawai, T. Fabrication of 0.5 nm electrode gaps using self-breaking technique. *Applied Physics Letters* **2008**, *93*, 163115.

(28) Caneva, S.; Gehring, P.; García-Suárez, V. M.; García-Fuente, A.; Stefani, D.; Olavarria-Contreras, I. J.; Ferrer, J.; Dekker, C.; van der Zant, H. S. J. Mechanically controlled quantum interference in graphene break junctions. *Nature Nanotechnology* **2018**, *13*, 1126–1131.

(29) Xie, P.; Xiong, Q.; Fang, Y.; Qing, Q.; Lieber, C. M. Local electrical potential detection of DNA by nanowire-nanopore sensors. *Nature Nanotechnology* **2012**, *7*, 119–125.

(30) Han, M. Y.; Özyilmaz, B.; Zhang, Y.; Kim, P. Energy Band-Gap Engineering of Graphene Nanoribbons. *Physical Review Letters* **2007**, *98*, 206805.

(31) Traversi, F.; Raillon, C.; Benameur, S. M.; Liu, K.; Khlybov, S.; Tosun, M.; Krasnozhon, D.; Kis, A.; Radenovic, A. Detecting the translocation of DNA through a nanopore using graphene nanoribbons. *Nature Nanotechnology* **2013**, *8*, 939–945.

(32) Puster, M.; Balan, A.; Rodríguez-Manzo, J. A.; Danda, G.; Ahn, J. H.; Parkin, W.; Drndic, M. Cross-Talk between Ionic and Nanoribbon Current Signals in Graphene Nanoribbon-Nanopore Sensors for Single-Molecule Detection. *Small* **2015**, *11*, 6309–6316.

(33) Heerema, S. J.; Vicarelli, L.; Pud, S.; Schouten, R. N.; Zandbergen, H. W.; Dekker, C. Probing DNA Translocations with Inplane Current Signals in a Graphene Nanoribbon with a Nanopore. *ACS Nano* **2018**, *12*, 2623–2633.

(34) Radisavljevic, B.; Radenovic, A.; Brivio, J.; Giacometti, V.; Kis, A. Single-layer MoS_2 transistors. *Nature nanotechnology* **2011**, *6*, 147–150.

(35) Farimani, A. B.; Min, K.; Aluru, N. R. DNA base detection using a single-layer MoS_2. *ACS Nano* **2014**, *8*, 7914–7922.

(36) Sarathy, A.; Leburton, J. P. Electronic conductance model in constricted MoS_2 with nanopores. *Applied Physics Letters* **2016**, *108*, 53701.

(37) Sarkar, D.; Liu, W.; Xie, X.; Anselmo, A. C.; Mitragotri, S.; Banerjee, K. MoS_2 field-effect transistor for next-generation label-free biosensors. *ACS Nano* **2014**, *8*, 3992–4003.

(38) Graf, M.; Lihter, M.; Thakur, M.; Georgiou, V.; Topolancik, J.; Ilic, B. R.; Liu, K.; Feng, J.; Astier, Y.; Radenovic, A. Fabrication and practical applications of molybdenum disulfide nanopores. *Nature Protocols* **2019**, *14*, 1130–1168.

(39) Parkin, W. M.; Drndić, M. Signal and Noise in FET-Nanopore Devices. *ACS Sensors* **2018**, *3*, 313–319.

(40) Kowalczyk, S. W.; Grosberg, A. Y.; Rabin, Y.; Dekker, C. Modeling the conductance and DNA blockade of solid-state nanopores. *Nanotechnology* **2011**, *22*, 315101.

(41) Vlassarev, D. M.; Golovchenko, J. A. Trapping DNA near a solid-state nanopore. *Biophysical Journal* **2012**, *103*, 352–356.

(42) Carlsen, A. T.; Zahid, O. K.; Ruzicka, J.; Taylor, E. W.; Hall, A. R. Interpreting the conductance blockades of DNA translocations through solid-state nanopores. *ACS Nano* **2014**, *8*, 4754–4760.

(43) Kwok, H.; Waugh, M.; Bustamante, J.; Briggs, K.; Tabard-Cossa, V. Long Passage Times of Short ssDNA Molecules through Metallized Nanopores Fabricated by Controlled Breakdown. *Advanced Functional Materials* **2014**, *24*, 7745–7753.

(44) Lu, C.; Liu, Y.; Ying, Y.; Liu, J. Comparison of MoS_2, WS_2, and graphene oxide for DNA adsorption and sensing. *Langmuir* **2017**, *33*, 630–637.

(45) Zhu, C.; Zeng, Z.; Li, H.; Li, F.; Fan, C.; Zhang, H. Single-Layer MoS_2 Based Nanoprobes for Homogeneous Detection of Biomolecules. *Journal of the American Chemical Society* **2013**, *135*, 5998–6001.

(46) Qiu, H.; Sarathy, A.; Schulten, K.; Leburton, J.-P. Detection and mapping of DNA methylation with 2D material nanopores. *npj 2D Materials and Applications* **2017**, *1*, 3.

(47) Graf, M. 2D nanopores: fabrication, energy harvesting and field-effect sensing. Ph.D. thesis, EPFL, Lausanne, VD, 2019.

(48) Schoch, R. B.; Han, J.; Renaud, P. Transport phenomena in nanofluidics. *Reviews of Modern Physics* **2008**, *80*, 839–883.

(49) Yoon, Y.; Ganapathi, K.; Salahuddin, S. How Good Can Monolayer MoS_2 Transistors Be? *Nano Letters* **2011**, *11*, 3768–3773.

(50) Smeets, R. M. M.; Keyser, U. F.; Dekker, N. H.; Dekker, C. Noise in solid-state nanopores. *Proceedings of the National Academy of Sciences* **2008**, *105*, 417–421.

(51) Singh, T.; Kumar, A. Static Dielectric Constant of Room Temperature Ionic Liquids: Internal Pressure and Cohesive Energy Density Approach. *The Journal of Physical Chemistry B* **2008**, *112*, 12968–12972.

(52) Gebbie, M. A.; Smith, A. M.; Dobbs, H. A.; Lee, A. A.; Warr, G. G.; Banquy, X.; Valtiner, M.; Rutland, M. W.; Israelachvili, J. N.; Perkin, S.; Atkin, R. Long range electrostatic forces in ionic liquids. *Chem. Commun.* **2017**, *53*, 1214–1224.

Graphical TOC Entry